Materials Research Proceedings 52 (2025) 242-249 https://doi.org/10.21741/9781644903551-30

A dieless Nakajima test for additively deposited materials

Rui F.V. Sampaio[1,a*], Pedro M.S. Rosado[1,b], João P.M. Pragana[1,c], Ivo M.F. Bragança[2,d], Chris V. Nielsen[3,e], Carlos M.A. Silva[1,f] and Paulo A.F. Martins[1,g]

[1]IDMEC, Instituto Superior Técnico, Universidade de Lisboa, Portugal

[2]CIMOSM, Instituto Superior de Engenharia de Lisboa, Instituto Politécnico de Lisboa, Portugal

[3]Department of Civil and Mechanical Engineering, Technical University of Denmark

[a]rui.f.sampaio@tecnico.ulisboa.pt, [b]pedro.s.rosado@tecnico.ulisboa.pt, [c]joao.pragana@tecnico.ulisboa.pt, [d]ibraganca@dem.isel.ipl.pt, [e]cvni@dtu.dk, [f]carlos.alves.silva@tecnico.ulisboa.pt, [g]pmartins.tecnico.ulisboa.pt

Keywords: Additive Manufacturing, Forming, Nakajima Test

Abstract. This paper focuses on a novel Nakajima test for characterizing the formability of additively deposited materials without extracting sheet blanks. Material is deposited by wire-arc additive manufacturing in the form of 'Π-shaped' vertical walls, and the testing regions are then machined to the desired thickness and shapes for subsequent deformation with a hemispherical punch in a press. Digital image correlation is used to obtain the strain loading paths of the deposited material up to failure. The novel test eliminates the need for the special-purpose tool setup of conventional Nakajima tests, simplifying the overall procedure and reducing costs.

Introduction

Combining metal additive manufacturing (MAM) with metal forming gives rise to new hybrid manufacturing routes that explore the advantages of both technologies to create high-quality parts with complex designs. Hybridization of MAM with metal forming can be used to introduce reinforcements [1] and functional elements [2] in parts, which would have been very difficult or impossible to obtain through traditional forming processes alone or, alternately, to produce preforms that are subsequently subjected to traditional sheet, bulk, and sheet-bulk forming processes to fabricate net-shape or near-net-shape parts in small to medium batch sizes [3].

However, the hybridization of MAM with metal forming suffers from anisotropy and formability problems [4] caused by the metallurgical structure of the deposited materials that often restrict its domain of applicability to low plastic deformation levels. This is particularly relevant to material deposited by wire-arc additive manufacturing (WAAM) rather than other MAM processes, and it justifies the paper's focus on WAAM-deposited materials.

WAAM is a form of wire-directed energy deposition (wire-DED) that utilizes an electric arc to provide the thermal energy necessary for melting and depositing the wire feedstock layer by layer and shares working principles with well-established gas metal arc, gas tungsten arc, or plasma arc welding processes. Its growing interest stems from its ability to create large-scale parts with low to medium quality due to its material efficiency and high deposition rates (5-6 kg/h) and due to the widespread availability of arc welding-based machines and motion systems in metalworking companies.

However, WAAM still faces difficulties meeting the parts' geometrical, surface, and metallurgical requirements due to the large melt pools created by the electric arc. These pools give rise to differential expansion and contraction across the deposited material during the heating and cooling cycles, as well as to porosity, precipitation reactions, and formation of dendritic-based columnar grain structures [5]. The latter is responsible for the above-mentioned reported difficulties related to anisotropy and formability limits.

This paper aims to characterize the formability of WAAM-deposited stainless steel by focusing on a novel dieless Nakajima testing procedure that was recently proposed by the authors [6]. In contrast to the conventional Nakajima setup shown in Fig. 1, the novel testing procedure is carried out directly on the deposited material without the need to extract sheet blanks or use the special purpose tool setup of conventional Nakajima tests, which typically involves a punch, a die, and a blank holder [7]. The design of the dieless Nakajima test is supported by finite element simulations, utilizing in-house software, and by experimentation employing digital image correlation (DIC) to obtain the strain loading paths up to failure in principal strain space. Material deposition by WAAM is simulated by finite elements using new modelling features of the in-house software.

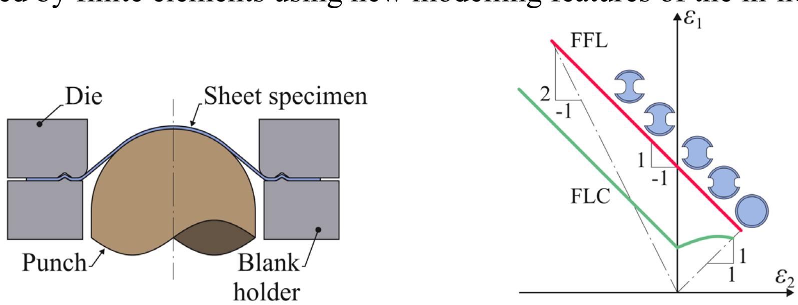

Fig. 1 Schematic representation of the conventional Nakajima test with illustration of the forming limit curve (FLC) and fracture forming line (FFL) in principal strain space obtained from different sheet blank geometries (adapted from [6]).

Experimentation

Material Deposition. The work was carried out in AISI 316L stainless steel deposited by WAAM using an ESAB Luc Aristo 400 gas metal arc welding power source coupled with a 3-axis CNC router table. The AISI 316L wire feedstock, with a diameter of 1.0 mm, was supplied through the welding torch and melted with a spray transfer mode onto hot rolled AISI 316L baseplates having 16 mm thickness.

Table 1 summarizes the main WAAM parameters used to construct the 'Π-shaped' vertical walls (hereafter referred to as 'deposited walls' or simply 'walls'). These parameters were retrieved from the authors' previous work [8], which used the same wire and baseplate materials to construct vertical walls under a stable electric arc.

Table 1 Summary of the WAAM processing parameters utilized in the deposition of AISI 316L.

Current [A]	Voltage [V]	Wire feed speed [m/min]	Travel speed [m/min]	Shielding gas	Gas flow rate [l/min]	Layer height [mm]
100	16.5	6	0.5	Argon 99.9%	10	1.8

The deposited walls with main dimensions shown in Fig. 2a were constructed through single-bead deposition layers along sequences with variable starting points at each layer to balance the heating and cooling cycles.

Dieless Nakajima Test. The dieless Nakajima test requires machining the web plates of the deposited walls to obtain a good-quality circular testing region of uniform thickness. In the current investigation, this region had a 1 mm thickness and 73.5 mm diameter at the center. Waterjet cutting was employed to modify the original circular geometry, which was aimed at providing equibiaxial strain loading paths, into an arc-shaped geometry, which was aimed at delivering near uniaxial strain loading paths. The overall test geometries were more compact, with a 0.7 size ratio compared to that recommended in the ISO 12004-2 standard.

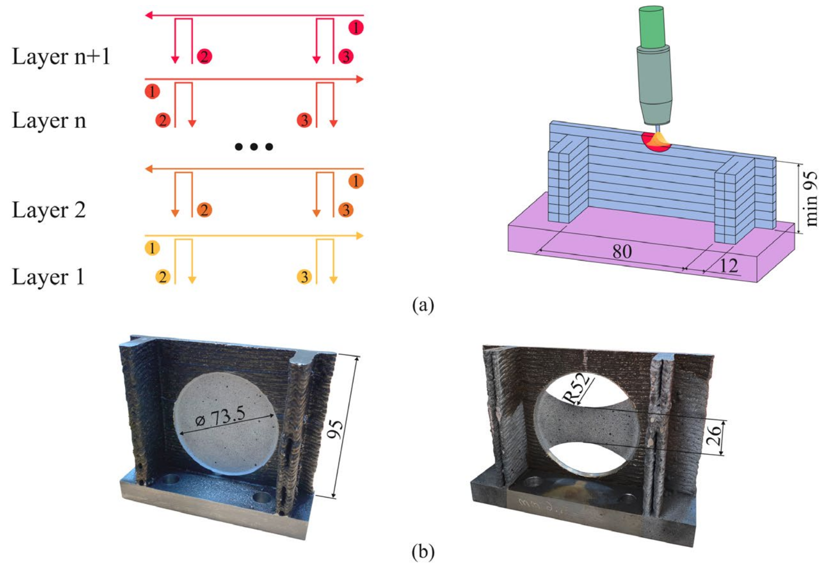

Fig. 2. (a) Schematic representation of the deposition strategy utilized in WAAM and (b) photographs of the deposited walls after machining the upper end and the central region to obtain circular and arc-shaped Nakajima test geometries (adapted from [6]).

The edges of the deposited walls were also machined perpendicularly to the building direction with good surface quality for subsequent fixing in the multidirectional tool, where the dieless Nakajima tests were performed (Fig. 3a). The tool converts the vertical crosshead movement of the hydraulic testing machine into the horizontal movement of a hemispherical punch with 70 mm diameter using a cam slide unit with a working angle $\alpha = 30°$ that consists of a sliding wedge actuator attached to the upper bolster. To minimize friction, a 0.5 mm Teflon sheet and molybdenum disulfide grease were added between the hemispherical punch and the testing region.

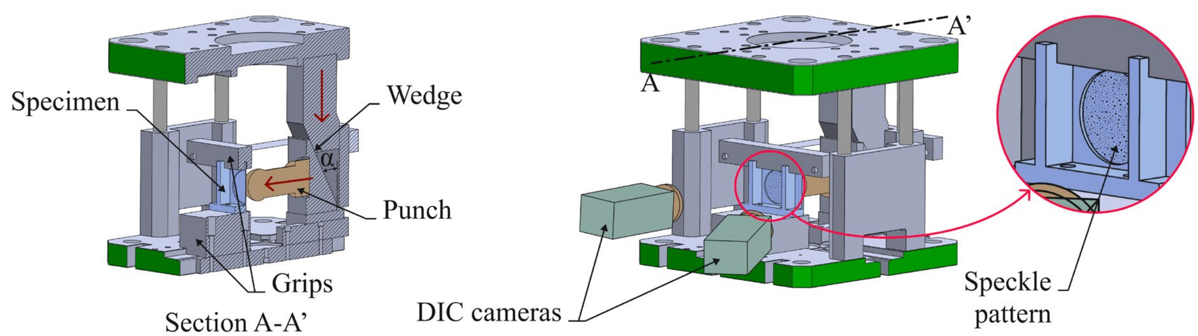

Fig. 3 Schematic representation of the dieless Nakajima testing setup in the multidirectional tool with detail of the setup used by the digital image correlation (DIC) system (adapted from [6]).

The side of the region of interest opposite to the hemispherical punch was painted white and, subsequently, with a stochastic black dot pattern (Fig. 3b) to ensure a reliable collection of the evolution of the in-plane strains over time $\varepsilon_1(t)$, $\varepsilon_2(t)$, using a commercial digital image correlation (DIC) system from Dantec Dynamics (model Q-400 3D). This system featured two 6-megapixel resolution cameras equipped with 50.2 mm focal length lenses and f/8 aperture (Fig. 3b), and the region of interest was illuminated by a spotlight during testing. Images were captured by the cameras at a shutter frequency of 10 Hz.

The authors' software [9] was utilized to merge the evolutions of in-plane strains over time $\varepsilon_1(t)$, $\varepsilon_2(t)$ into strain loading paths $\varepsilon_1 = f(\varepsilon_2)$ in principal strain space by removing the time dependency.

Materials Research Proceedings 52 (2025) 242-249 https://doi.org/10.21741/9781644903551-30

Numerical Simulation

The numerical simulation of material deposition by WAAM and Nakajima testing was carried out using the in-house computer program I-FORM. In the case of WAAM, the approach involved the transformation of the non-linear thermo-mechanical macro-scale model into a staggered sequential solution of the heat transfer (1) and the quasi-static equilibrium (2) equations (under the absence of body forces) within a time increment Δt,

$$k\nabla^2 T - \rho c \frac{\partial T}{\partial t} + \dot{q} = 0 \,. \tag{1}$$

$$\frac{\partial \sigma_{ij}}{\partial x_j} = 0 \,. \tag{2}$$

In the above equations, k represents the thermal conductivity, ρ stands for the mass density, c denotes the specific heat capacity, $\dot{q}$ is the total input power density, σ_{ij} represents the Cauchy stress tensor, and x_j denotes an arbitrary position within the baseplate and deposited material at the current instant of time t. The total power density $\dot{q}$ in (1) is approximated through a heat source model, which in the current software implementation consists of the asymmetric Gaussian moving double-ellipsoid proposed by Goldak et al. [10], because it effectively accounts for the total power transferred to both filler and baseplate materials.

The thermal loads induced by temperature changes within a time increment Δt are included in the solution of the quasi-static equilibrium equations (2) through a thermal strain increment $\Delta\varepsilon^t = \alpha(T)\Delta T$, where the symbol α denotes the coefficient of thermal expansion. The thermal strain increment $\Delta\varepsilon^t$ is then combined with the elastic strain increment $\Delta\varepsilon^e$, calculated from the elasticity modulus and Poisson ratio, and the plastic strain increment $\Delta\varepsilon^p$ determined from the material flow curve to obtain the total increment of strain $\Delta\varepsilon = \Delta\varepsilon^e + \Delta\varepsilon^p + \Delta\varepsilon^t$ and the distribution of stresses, through the constitutive equation,

$$\sigma_{ij} = C_{ijkl}(\varepsilon_{kl} - \varepsilon_{kl}^p - \varepsilon_{kl}^t) \,. \tag{3}$$

where the symbol C_{ijkl} denotes the fourth order material stiffness tensor.

Fig. 4a provides a detailed view of the model used in the numerical simulation of material deposition by WAAM. The baseplates were clamped to a table to minimize distortion, and the clamps were included in the finite element model using single node constraints of the baseplates' left and right bottom surface edges. The remaining surfaces of the model were assigned with free convection boundary conditions with convection coefficient values equal to 15 (W/m^2K) and radiation to the environment. The model consisted of approximately 70,000 hexahedral elements active at the end of the deposition, with mechanical and physical properties assumed to be temperature dependent. A ‘born-dead element’ variant of the ‘element birth’ technique, where new mesh elements are gradually activated as the heat source moves to simulate the formation, detachment, and impingement of droplets from the filler material into the molten pool was utilized.

Macro-scale modeling approach of WAAM was validated in a previous work of the authors [11], which used the same material and revealed an excellent agreement between numerically predicted and experimentally measured temperatures, and between numerically predicted and experimentally measured distortions after cooling and unclamping the baseplates.

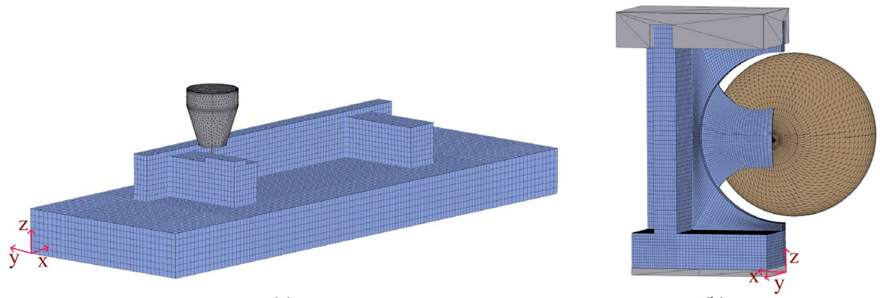

Fig. 4 Finite element model of the (a) material deposition by WAAM and (b) dieless Nakajima test performed with an arc-shape geometry after some hemispherical punch displacement.

The numerical simulation of the Nakajima test made use of the finite element flow formulation built upon the quasi-static equilibrium equations (2). The model treated the deposited walls as deformable objects, and the material was assumed as isotropic, following the Levy-Mises constitutive equations. The flow stress (4) was determined by averaging the values obtained for the transverse, longitudinal, and inclined directions in a previous study of the authors [8],

$$\sigma = 1200\varepsilon^{0.35}\ (\mathrm{MPa})\,. \tag{4}$$

Fig 4b shows a typical model considering a symmetrical plane and discretizing the deposited walls with approximately 50,000 three-dimensional hexahedral elements. The discretization is more refined at the center of the region of interest, where the hemispherical punch first contacts the deposited material.

The hemispherical punch and the grips holding the upper end of the deposited walls were assumed to be rigid objects and discretized using spatial triangular elements. The Prandtl law of constant friction was utilized between the rigid objects and the deposited walls, with the friction factor at the contact with the punch and the lower bolster of the multidirectional tool being respectively equal to 0.1 and 1.0. The first value accounted for the Teflon sheet placed in the region of interest. In contrast, the second value allowed the model to accurately replicate the fixing of the odd-sized deposited walls to the lower bolster through bolts.

Results and Discussion

Temperature and Temperature Gradients in WAAM. Figs. 5a and 5b show the finite element predicted distribution of temperature and temperature gradient at an instant of material deposition corresponding to the tenth layer. The maximum temperature is capped at the melting temperature (approximately equal to 1400˚C) to facilitate the identification of the molten pool, and the temperature distribution discloses contours that gradually increase at the front and rear of the molten pool, in agreement with the asymmetric Gaussian distribution of heat flux.

Reheating caused by deposition of the different layers combined with the heat flow into the baseplate, which remains cooler, gives rise to a temperature gradient that is maximum where material is being deposited and aligned with the building height. This alignment closely mirrors the orientation of the primary arms of dendritic growth along the building direction (Fig. 5c), and it is crucial for understanding the formation of columnar grain-based microstructures and the highly anisotropic behavior of the material deposited by WAAM.

Materials Research Proceedings 52 (2025) 242-249 https://doi.org/10.21741/9781644903551-30

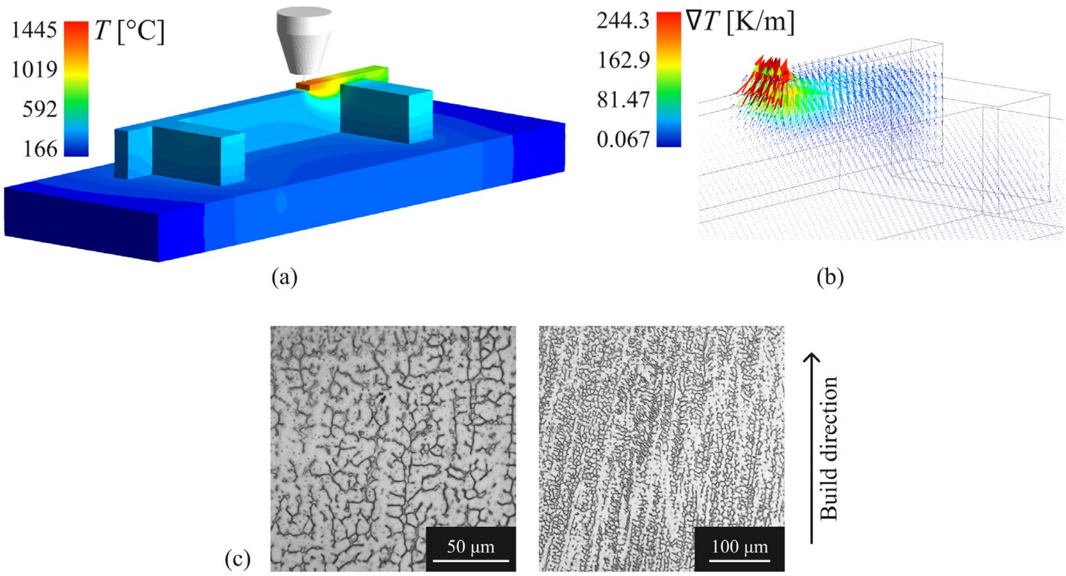

Fig. 5 Finite element predicted distribution of (a) temperature and (b) temperature gradient during deposition of the tenth layer of the main wall. (c) Microstructure observation of a sample extracted from the main wall.

Structural Integrity of the Dieless Nakajima Setup. The finite element predicted effective strain distributions after 20 mm punch displacement for the circular and arc-shaped test geometries shown in Fig. 6 demonstrate that the deposited walls outside the area of interest possess sufficient strength to maintain their original structural integrity. Their function is akin to the die and blank holder of the blank sheet, which is mimicked by the thinner machined region of interest undergoing plastic deformation due to contact with the hemispherical punch.

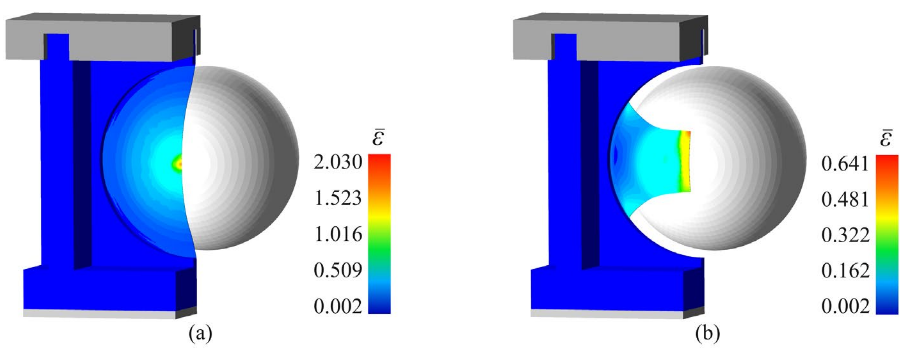

Fig. 6 Finite element predicted distribution of effective strain after 20 mm punch displacement for the (a) circular and (b) arc-shaped test geometries.

Strain Loading Paths and Failure. Fig. 7a shows the finite element predicted accumulation of ductile damage according to the McClintock ductile fracture criterion [12] for the circular and arc-shaped test geometries in case of assuming the material as isotropic. Higher damage values accumulate at the center of the region of interest, in contact with the hemispherical punch pole, validating the new procedure as an alternative to conventional Nakajima tests using toolsets with a punch, a die, and a blank holder.

The utilization of the previously mentioned software [9] to obtain the strain loading paths $\varepsilon_1 = f(\varepsilon_2)$ in principal strain space from DIC measurements gave the results shown in Fig. 7b In both test geometries, the open markers represent the final DIC measurements on the area where the crack was triggered, whereas the solid markers denote the in-plane strains at the fracture. The latter were obtained from thickness measurements along the crack to obtain the thickness strains given

Materials Research Proceedings 52 (2025) 242-249 https://doi.org/10.21741/9781644903551-30

by $\varepsilon_3 = ln(t_f/t_o)$, where t_o is the initial thickness and t_f is the thickness at fracture, assuming no changes in the minor strain $\Delta\varepsilon_2 = 0$ after the last DIC measurement.

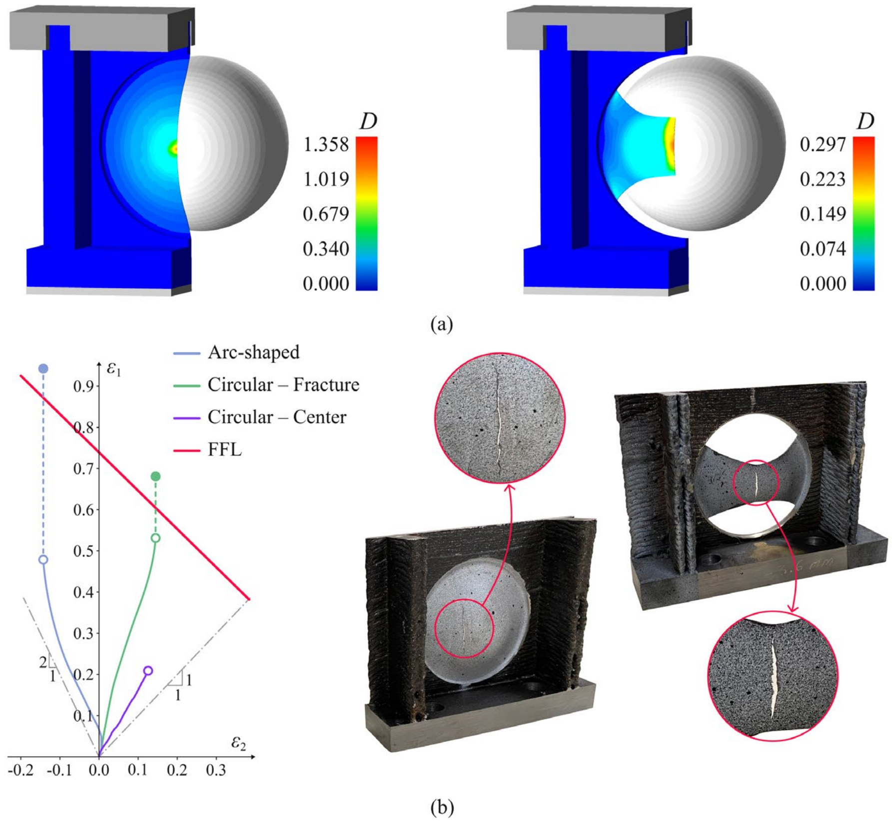

Fig. 7 (a) Finite element predicted distribution of ductile damage according to the McClintock fracture criterion after 20 mm punch displacement for the circular and arc-shaped test geometries. (b) Strain loading path evolutions with pictures of both test samples after failure.

In the case of the circular test geometry, two locations were chosen, corresponding to the center and the zone where the crack was triggered. The strain loading paths corresponding to these two locations are different and confirm the position of the crack slightly shifted away from the center (Fig. 7c) and in close agreement with the fracture forming limit (FFL) of this material that the authors previously determined [8] (refer to the red line in Fig. 7c).

The crack shift in the circular test geometry is attributed to the combined effect of friction and anisotropy. Even with a Teflon sheet between the hemispherical punch and the region of interest, friction carries part of the in-plane loads and allows cracks to initiate at the edge of the tool contact, away from the center. Anisotropy, caused by the dendritic-based columnar grain microstructure of the deposited walls, contributes to the cracks' alignment with the building direction.

Conclusions

The dieless Nakajima test enables direct characterization of the formability limits of deposited materials without extracting sheet blanks. The results obtained with circular and arc-shaped geometries confirm the validity of the proposed design, which utilizes the surrounding material of the region of interest to replicate the die and blank holder, ensuring strain loading paths similar to those obtained in conventional Nakajima sheet formability tests.

Macro-scale thermo-mechanical modeling of WAAM, performed independently from the formability test modelling, predicts vertical temperature gradients that closely mirror the orientation of dendritic growth along the building direction, which leads to a general anisotropic behavior of the deposited materials. This behavior, together with good lubrication leads to a shift of cracks away from the center of the region of interest in the case of circular geometry.

Acknowledgements
The authors would like to acknowledge the support provided by Fundação para a Ciência e a Tecnologia (FCT) and IDMEC for its financial support via the project LAETA Base Funding (DOI: 10.54499/UIDB/50022/2020).

References

[1] M. Bambach, A, Sviridov, A. Weisheit, J.H. Schleifenbaum, Case studies on local reinforcement of sheet metal components by laser additive manufacturing, Metals 7 (2017) 113. https://doi.org/10.3390/met7040113

[2] M. Merklein, D. Junker, A. Schaub, F. Neubauer, Hybrid additive manufacturing technologies - An analysis regarding potentials and applications, Phys. Procedia 83 (2016) 549-559. https://doi.org/10.1016/j.phpro.2016.08.057

[3] J.P.M. Pragana, R.F.V. Sampaio, I.M.F. Bragança, C.M.A. Silva, P.A.F. Martins, Hybrid metal additive manufacturing: A state-of-the-art review, Adv. Ind. Manuf. Eng. 2 (2021) 100032. https://doi.org/10.1016/j.aime.2021.100032

[4] C. López, A. Elías-Zúñiga, I. Jiménez, O. Martínez-Romero, H.R. Siller, J.M. Diabb, Experimental determination of residual stresses generated by single point incremental forming of AlSi10Mg sheets produced using SLM additive manufacturing process, Materials 11 (2018) 2542. https://doi.org/10.3390/ma11122542

[5] A Shah, R. Aliyev, H. Zeidler, S. Krinke, A review of the recent developments and challenges in wire arc additive manufacturing (WAAM) process, J. Manuf. Mater. Process. 7 (2023) 97. https://doi.org/10.3390/jmmp7030097

[6] R.F.V. Sampaio, P.M.S. Rosado, J.P.M. Pragana, I.M.F. Bragança, C.M.A. Silva, L.G. Rosa, P.A.F. Martins, Formability assessment of additively manufactured materials via dieless Nakajima testing, J. Manuf. Mater. Process. 8 (2024) 180. https://doi.org/10.3390/jmmp8040180

[7] K. Nakajima, T. Kikuma, K. Hasuka, Study on the Formability of Steel Sheets, Yamata Technical Report, Japan, 1968.

[8] J.P.M. Pragana, I.M.F. Bragança, L. Reis, C.M.A. Silva, P.A.F. Martins, Formability of wire-arc deposited AISI 316L sheets for hybrid additive manufacturing applications, Proc. Inst. Mech. Eng. Part L J. Mater. Des. Appl. 235 (2021) 2839-2850. https://doi.org/10.1177/14644207211037033

[9] R.F.V. Sampaio, N.S.M. Alexandre, J.P.M. Pragana, I.M.F. Bragança, C.M.A. Silva, P.A.F. Martins, A software for research and education in ductile damage, Adv. Ind. Manuf. Eng. 7 (2023) 100127. https://doi.org/10.1016/j.aime.2023.100127

[10] J. Goldak, A. Chakravarti, M.A. Bibby, A new finite element model for welding heat sources, Metall. Trans. B 15 (1984) 299-305. https://doi.org/10.1007/BF02667333

[11] J.P.M. Pragana, R.F.V. Sampaio, I.M.F. Bragança, C.M.A. Silva, C.V. Nielsen, P.A.F. Martins, Macro-scale finite element simulation of wire-arc additive manufacturing, Proc. Inst. Mech. Eng. Part L J. Mater. Des. Appl. (2024) (in press). https://doi.org/10.1177/14644207241272840

[12] F.A. McClintock, A criterion for ductile fracture by the growth of holes, J. Appl. Mech. 35 (1968) 363-371. https://doi.org/10.1115/1.3601204